Academic Journal of Science and Technology
ISSN: 2771-3032 | Vol. 10, No. 1, 2024

Grinding Force Model and Experimental Study on Ultrasonic Assisted Spiral Grinding of Silicon Carbide Ceramic Materials

Chongyang Zhao[1,*], Chenyu Liang[1], Xiaobo Wang[1], Yi Wang[1], Jishan Han[1]

[1] Henan Polytechnic University, Jiaozuo, China

[*] Corresponding author: Chongyang Zhao (Email: zhaocy@hpu.edu.cn)

Abstract: In order to reveal the mechanical properties of silicon carbide ceramic materials during the drilling process, based on the indentation fracture mechanics theory, a grinding force model of ultrasonic assisted spiral grinding for hole making was established, and the experimental results of ultrasonic assisted spiral grinding for hole making verified the mechanical model. The results showed that the experimental results had the same change trend as the predicted results of the established mechanical model, and the values were close to each other, indicating the accuracy of the established prediction model. The influence of different process parameters on the size accuracy of the hole inlet and outlet aperture after machining is analyzed. It is found that it should be selected as large rotation speed, moderate axial feed speed and small feed pitch to ensure the accuracy of the aperture and effectively suppress the aperture defects during ultrasonic assisted spiral grinding.

Keywords: Ultrasonic assisted spiral grinding, Silicon carbide ceramics, Grinding force model, Size accuracy of aperture.

1. Introduction

Silicon carbide ceramic materials have high hardness, high strength, high modulus physical properties, corrosion resistance ,high temperature resistance, and wear resistance chemical properties [1-2], these advantages make it have a very unique advantage in aerospace, nuclear industry ,brake system and other industries, but due to the mechanical properties of silicon carbide ceramic materials anisoanisoy, poor thermal conductivity. It is a typical material that could result in extremely harsh processing conditions combined with low strength characteristics. At present, the common processing methods of silicon carbide ceramic materials mainly fall into two categories: traditional processing and special processing. In the traditional grinding process, the grinding force is large and the tool wear is serious. In the processing process, a new type of tool needs to develop to improve the tool life [3]. Common special machining includes rapid prototyping, laser machining, abrasive water jet machining, electric discharge machining and ultrasonic assisted machining. This paper mainly studies the grinding force of ultrasonic assisted spiral grinding of silicon carbide ceramic materials. Taking silicon carbide ceramic materials as the research object, the grinding force model of longitudinal-torsional combined ultrasonic vibration assisted spiral grinding is established, the experimental platform is set up, the model is verified through experiments, and the dimensional accuracy of the aperture is analyzed, and the influence of main process parameters on the dimensional accuracy of the aperture is analyzed. The experimental results show that ultrasonic assisted spiral grinding can effectively improve the aperture quality of silicon carbide ceramic materials. Ultrasonic assisted spiral grinding plays a significant role in improving tool processing conditions, increasing tool service life and improving machining efficiency.

2. Dynamic Analysis of Ultrasonic Assisted Spiral Grinding

2.1. Principle of hole making

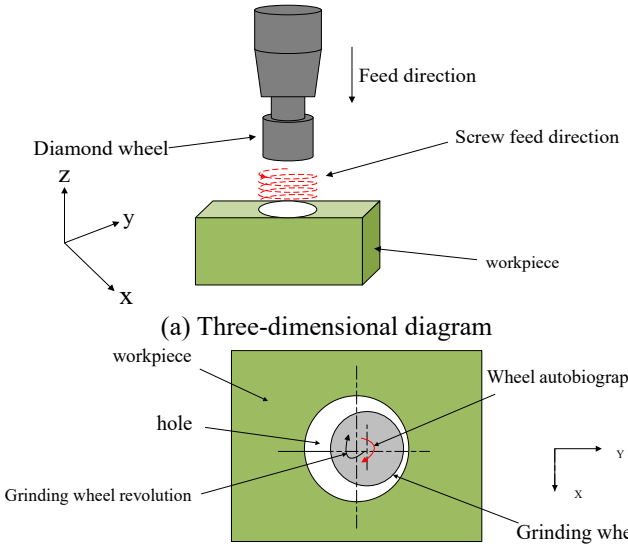

(a) Three-dimensional diagram

(b) Z direction schematic diagram

Figure 1. Principle of Ultrasonic Assisted Spiral Grinding Hole Making

The machining mode of ultrasonic assisted helical grinding for hole making is shown in Figure **1.** The tool moves along the helix at a certain feed speed under the combined action of the workpiece feed movement along the O-XY plane and the tool feed movement along the Zaxis. Applying longitudinal vibration to the tool in the axial direction and torsional vibration in the normal direction, the tool rotates with the spindle and there is a certain distance between the central axis of the tool and the central axis of the workpiece, so that the tool is subjected to longitudinal torsional ultrasonic vibration at the same time of screw feed, and the spiral grinding hole of

the tool is realized.

2.2. Kinematics analysis of a single abrasive particle

In order to analyze the cutting behavior of abrasive particles in ultrasonic vibration assisted spiral grinding, a coordinate system was established with the center of machining hole on the upper surface of the workpiece as the origin. Assuming that the workpiece is relatively stationary, the motion path of the tool can be broken down into four kinds: one is the ultrasonic vibration along the axis, the second is the feed movement along the axis, the third is the rotation of the tool, and the last is the revolution of the tool around the center axis of the hole on the xoy plane. The motion mode of the tool is shown in Figure 2. Therefore, in the ultrasonic spiral grinding process, the motion trajectory of the abrasive particles on the grinding needle is expressed in the coordinate system as follows:

$$\begin{cases} x(t) = \dfrac{D-d}{2}\cos\dfrac{\pi n_1 t}{30} + \dfrac{d}{2}\cos\dfrac{\pi n_2 t}{30} \\ y(t) = \dfrac{D-d}{2}\sin\dfrac{\pi n_1 t}{30} + \dfrac{d}{2}\sin\dfrac{\pi n_2 t}{30} \\ z(t) = -v_f t + A\sin(2\pi f t) \end{cases} \tag{1}$$

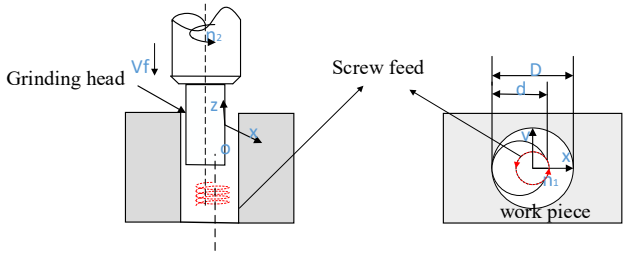

Figure 2. Schematic diagram of ultrasonic spiral grinding

2.3. Single abrasive cutting thickness model

Motion path of abrasive particles is shown in figure 3 and figure 4. In the process of ultrasonic assisted spiral grinding, the motion of abrasive particles without ultrasonic vibration in the horizontal direction includes the rotating motion of the grinding wheel around the hole axis and the rotating motion of the grain around the sand wheel axis, and in the vertical direction, the motion of abrasive particles is accompanied by the axial feed of the grinding wheel. In general, most of the particles are irregular polyhedrons. In order to facilitate analysis and calculation, a large number of scholars simplified the particles into cones in the modeling process [3,4,5], as shown in Figure 5, where the diameter of a single abrasive particle is Dg, Dg =100μm,$hg = \sqrt{3}Dg/3$, $\theta m = \pi/6 rad$. As shown in Figure 5, the grain distribution on the end face of the grinding wheel is uniform. On an arc of radiusR_i, As shown in Figure 5, the grain distribution is uniform on the end face of the grinding wheel. On an arc of radius R_i, the center Angle between the n particle Mn and the n+1 particle Mn+1 is ΦMn. The cutting thickness of abrasive particles is shown in figure. 6, and the arc length between two adjacent abrasive particles can be expressed as:

$$l_M = R_i \bullet \Phi_{Mn} \tag{2}$$

In the XOZ plane, the Angle between the horizontal feed velocity of the abrasive particles and the resultant velocity can be expressed as:

$$\tan\delta = \frac{D_2E_2}{A_2D_2} = \frac{h_M}{l_M} = \frac{V_{M2}}{V_{M1}} = \frac{Vfa}{Vc - Vft} \tag{3}$$

Because the spindle speed is much higher than the screw feed speed, the screw feed speed can be ignored and only the influence of the spindle speed can be considered. Equation (3) can be simplified as:

$$\tan\delta = \frac{h_M}{l_M} = \frac{V_{fa}}{V_c} = \frac{V_{fa}}{2\pi R_i n} \tag{4}$$

Different numbers of particles are distributed on arcs of different radii， Suppose that the number of R_{ki} particles on the arc isN_k.

when $0 < R_{k(i,j)} < d/2$, The number of particles on the arc of R_{ki} can be expressed as N_k :

$$N_k = \frac{R_{ki}}{l_M} \tag{5}$$

The average central Angle between adjacent particles can be expressed as Φ_{Ma} :

$$\Phi_{Ma} = \frac{2\pi}{Na} \tag{6}$$

From formula (3) ~ (6), it can be deduced that the theoretical wear particle thickness can be expressed as h_M :

$$h_M = \frac{v_{fa}}{n\sum_{k=1}^{k}(N_k \bullet n_k)} \tag{7}$$

It is assumed that the grinding cross-sectional areas of adjacent grains are the same, as shown in Figure 7. The cross-sectional area is S_M :

$$S_M = S_{ABCD} + S_{ADEF} + S_{BCJK} = \left(\frac{d_M}{2\tan\theta_M} - hg\right)\bullet h_M + h_M \bullet d_M \tag{8}$$

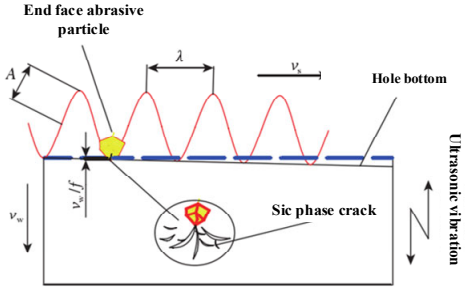

Figure 3 Transverse abrasive motion path

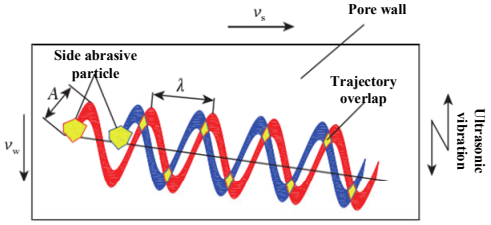

Figure 4 Side abrasive motion path

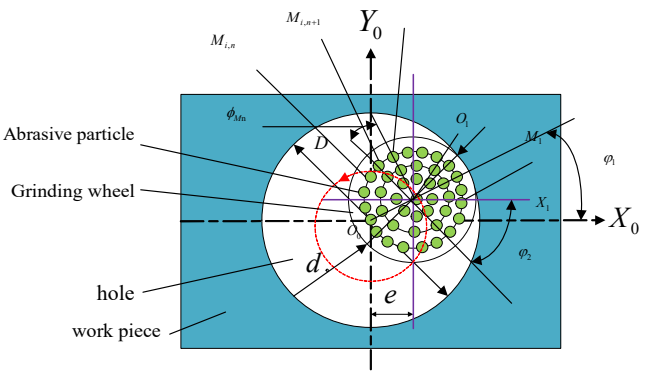

Figure 5 Geometric characteristics of grain movement on end face of grinding wheel

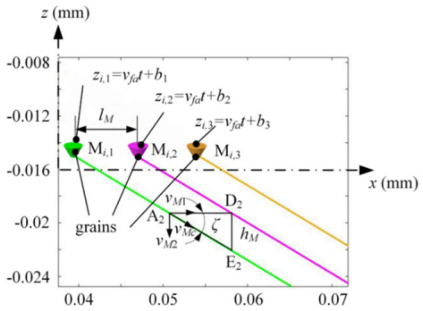

Figure 6 Grinding thickness chart

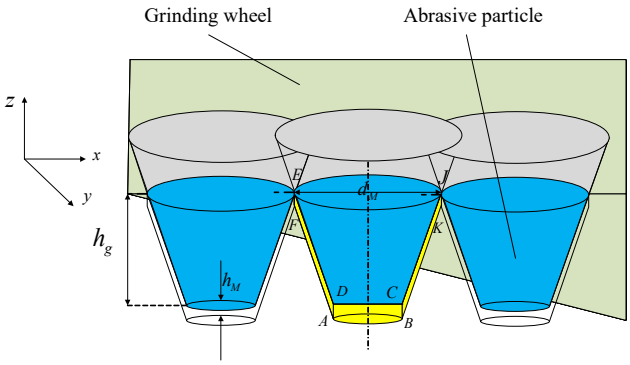

Figure 7 Grinding area diagram

2.4. Average cutting force model of a single abrasive particle

Under the action of ultrasonic vibration, wear particles continuously impact the workpiece material and produce a certain indentation depth. According to the theory of indentation fracture mechanics, the relationship between the impact force Fn of a single wear particle on the workpiece and the cutting depth δ within one ultrasonic vibration cycle is expressed [6] :

$$Fn = \frac{1}{2}\xi\delta^2(\tan\beta)Hv \tag{9}$$

Where, ξ is the geometric factor of abrasive pressure head, ξ=1.8544.

In one cycle, the effective time of the interaction between the abrasive particle and the material is t :

$$t = \frac{1}{\pi f}[\frac{\pi}{2} - \arcsin\theta(1-\frac{\delta}{A})] \tag{10}$$

Replacing the trajectory wave line of the action of abrasive particles on the material with a triangular wave, it can be simplified as:

$$t = \delta / 2Af \tag{11}$$

According to the impulse theorem, the average cutting force of a single abrasive particle in an ultrasonic cycle is Fc :

$$Fc = \gamma \cdot Fn \cdot f \cdot t \tag{12}$$

Where, γ is the impact waveform coefficient, and the triangular wave value is 0.5.

The theoretical material removal volume of a single abrasive particle in one ultrasonic cycle is V_0 :

$$V_0 = \frac{1}{3}\pi C_L C_h L \tag{13}$$

Among them, the distance of a single abrasive particle scratched on the workpiece surface in one ultrasonic cycle is $_L$:

$$L = \int_{t_1}^{t_2}[\frac{\pi rn}{30} + 2\pi fB\cos(2\pi ft + \varphi)]dt \tag{14}$$

Simplify to:

$$L = \frac{\pi rn\delta}{60Af} - \frac{2B\delta}{A}\sin\varphi \tag{15}$$

Marshall et al. [7] studied the lateral crack and obtained the expression of the lateral crack length C_L and depth C_h :

$$C_L = C_2(\frac{1}{\tan\beta})^{\frac{5}{12}}[\frac{E^{\frac{3}{4}}}{HvK_{IC}(1-v^2)^{\frac{1}{2}}}]^{\frac{1}{2}}Fn^{\frac{5}{8}} \tag{16}$$

$$C_h = C_2(\frac{1}{\tan\beta})^{\frac{1}{3}}\frac{E^{\frac{1}{2}}}{Hv}Fn^{\frac{1}{2}} \tag{17}$$

Where, K_{IC} is the fracture toughness of the material, $_E$ is the elastic modulus of the material, Hv is the hardness of the material, $_v$ is the Poisson ratio of the material, F_n is the force of the abrasive particle on the work, C_2 is a dimensionless constant with the value C_2 =0.226, β is the half top cone Angle of a single abrasive particle.

According to the definition of abrasive concentration, the effective number of abrasive particles on the end face of the tool can be obtained as Na [8] :

$$Na = C_0 \frac{c_a^{\frac{2}{3}}}{4sa^2}\pi(D_0^2 - D_i^2) \tag{18}$$

According to formula (12) and (18), the grinding force of the tool can be obtained as F_m :

$$F_m = \gamma \cdot F_n \cdot t \cdot f \cdot N_a \tag{19}$$

In summary, the expression of the cutting depth of a single abrasive particle can be expressed as:

$$\delta = \left[\frac{180MRRH_v^{\frac{3}{8}} K_{lc} \frac{1}{2}(1-v^2)^{\frac{1}{4}} A\tan\beta}{k(\frac{\xi}{2})^{\frac{9}{8}} c_2^2 Na\pi E^{\frac{7}{8}}(\pi rn - 120Bf\sin\varphi)} \right]^{\frac{4}{13}} \tag{20}$$

The grinding force experienced by the tool can be expressed as F_m :

$$F_m = \left[\frac{90(e+\frac{D_0}{2})^2 K_{lc}^{\frac{1}{2}}(1-v^2)^{\frac{1}{4}}}{kec_2^2\pi E^{\frac{7}{8}}(\pi rn - 120Bf\sin\varphi)} \right]^{\frac{12}{13}} (\frac{1}{2})^{\frac{51}{26}} \xi^{\frac{-1}{26}} (\tan\beta)^{\frac{62}{13}} H^{\frac{35}{26}} A^{\frac{-1}{13}} Na^{\frac{1}{13}} a_p^{\frac{12}{13}} v_f^{\frac{12}{13}} \tag{21}$$

3. Experimental Research on Cutting Force of Ultrasonic Assisted Spiral Grinding of Silicon Carbide Ceramic Materials

3.1. Experimental scheme

In order to verify the correctness of the established cutting force model and analyze the degree of influence of different process parameters on the cutting force of ultrasonic assisted spiral grinding, ultrasonic assisted spiral grinding hole experiments were carried out. The experimental devices mainly included CNC machine tools, ultrasonic vibration devices, force measuring systems, tools and workpieces, and the experimental system devices were shown in Figure 9. In this experimental system, the ultrasonic signal generated by the ultrasonic power supply is transmitted to the transducer through the wireless transmission disk, and the amplitude is amplified and transmitted to the tool through the amplitude transformer. The experiment was carried out on VMC850 machine tool. In the experiment, Kistle triaxial tester, 5057 multi-channel charge amplifier and computer were used to measure the grinding force dynamically. The grinding force data output by the force measuring system is analyzed by computer software. The validity of the grinding force model is verified by a set of single factor tests, and the influence of different process parameters on grinding force can be analyzed by the experimental results. The test parameters are shown in Table 1, the silicon carbide ceramic material used in the experiment is shown in Figure 10, the size is 20cm×20cm×5cm, and the basic parameters of the material are shown in Table 2.

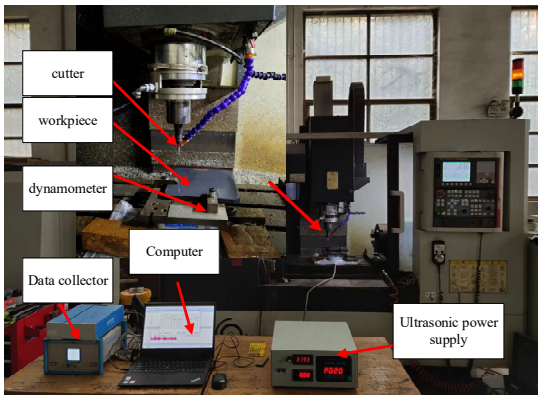

Figure 9. Experimental system diagram

Figure 10. Experiment material diagram

Table 1. Experiment parameters for model verification

Group number	Ultrasonic amplitude $A/\mu m$	Screw feed speed V_f /（mm/min）	Spindle speed n/（r/min）	Screw pitch a_p/mm
1	2.5	500	6000	1
1	3	500	6000	1
1	3.5	500	6000	1
1	4	500	6000	1
1	4.5	500	6000	1
2	3.5	450	6000	1
2	3.5	500	6000	1
2	3.5	550	6000	1
2	3.5	600	6000	1
2	3.5	650	6000	1
3	3.5	500	5000	1
3	3.5	500	5500	1
3	3.5	500	6000	1
3	3.5	500	6500	1
3	3.5	500	7000	1
4	3.5	500	6000	0.5
4	3.5	500	6000	1
4	3.5	500	6000	1.5
4	3.5	500	6000	2
4	3.5	500	6000	2.5

Table 2. Basic parameters of materials

Density g/cm^3	Bending strength Mpa	Compressive strength Mpa	Tensile Strength Mpa	Fracture Toughness Mpa·m$^{1/2}$
2.26	443.8	454	271.4	24.1

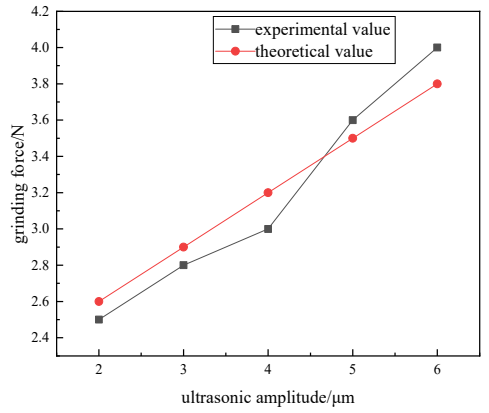

(a)

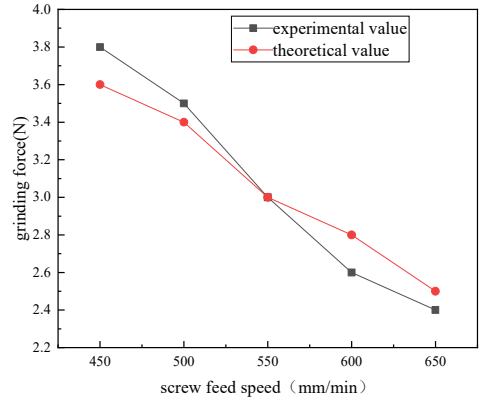

(b)

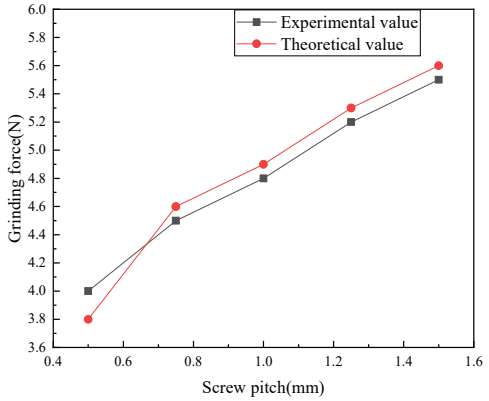

(c)

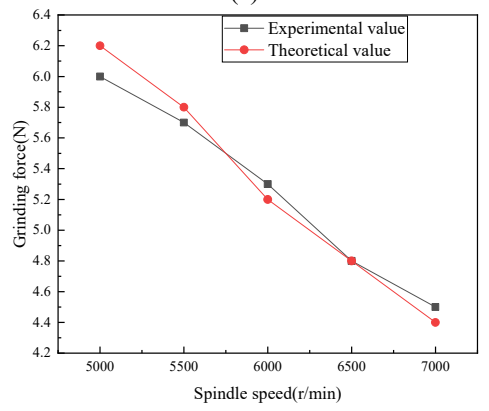

(d)

Figure. 11 Influence of different process parameters on grinding force

3.2. Analysis of experimental results

Figure. 11 respectively shows the comparison between ultrasonic amplitude, spiral feed speed, pitch and spindle speed theoretical values and experimental results. It can be seen from the figure that there is little difference between experimental values and theoretical values, which verifies the accuracy of the grinding force model. It can be seen from the figure that the influence law of different process parameters on the experimental results. It can be seen in Figure 11(a) that the grinding force decreases with the increase of ultrasonic amplitude. This is because with the increase of ultrasonic amplitude, the contact area between the particle and the workpiece becomes larger, the cutting volume per unit time increases, and the effective cutting time decreases, resulting in a decrease in grinding force. When the amplitude is before 2-4.5μm, the experimental value is less than the theoretical value, mainly because the ultrasonic amplitude is small and the influence on the grinding force is small. With the increase of the amplitude, the influence degree of the amplitude on the grinding force is increasing, resulting in the phenomenon that the experimental value is greater than the theoretical value.

It can be seen from Figure. 11 (b) that the grinding force increases with the increase of the screw feed speed. This is because the increase of the screw feed speed increases the material removal rate, thus increasing the grinding force. It can be seen from Figure 11 (c) that the grinding force gradually increases with the increase of the pitch, because the increase of the pitch essentially increases the cutting depth of the abrasive particle, and the amount of material removal per unit time also increases correspondingly, thus increasing the grinding force. It can be seen from Figure. 11 (d) that the grinding force decreases with the increase of the spindle speed. This is because the increase of the spindle speed increases the number of abrasive particles involved in grinding per unit time, resulting in a decrease in the cutting amount of materials by a single abrasive particle. At the same time, it is also conducive to the formation of smaller chips in time to discharge the processing area, reduce tool wear, etc., so as to effectively reduce the cutting force.

3.3. Dimensional accuracy analysis of holes in ultrasonic assisted spiral grinding of Silicon carbide ceramic matrix composites

3.3.1. The influence of speed on the dimensional accuracy of aperture

Figure. 12 shows the change curve of measured inlet and outlet diameters of holes with different eccentricities along with spindle speed. It can be seen from Figure. 3 that the inlet diameter of the holes processed in the three experiments is larger than the outlet diameter. Based on the movement law of spiral grinding holes, the main reason that the inlet diameter of the holes is larger than the outlet diameter is caused by the constant wear of the tool and the elastic deformation of the workpiece caused by the vibration of the tool during the machining process of the holes. Under the same eccentricity, the diameter of the entrance and outlet of the hole decreases first and then increases with the change of

the grinding head speed, mainly because the axial force and radial force decrease first and then increase with the increase of the rotating speed during the machining process.

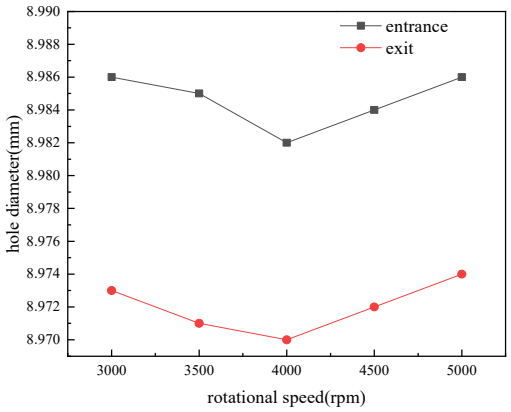

(a) e=0.5mm

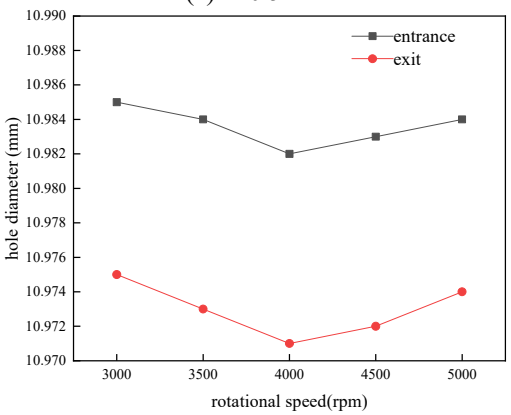

(b) e=1mm

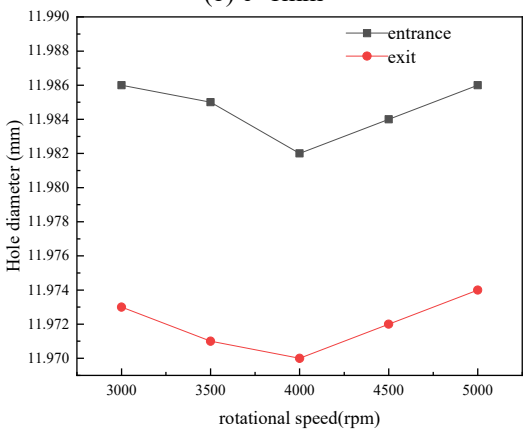

(c) e=1.5mm

Figure.12 Influence of spindle speed on aperture under different eccentricity

3.3.2. The influence of axial feed speed on the dimensional accuracy of the aperture

Figure 13 shows the change curve of hole inlet and outlet diameters measured under different eccentricities along with the axial feed speed. It can be seen from Figure.4 that under the same eccentricity, the diameter of hole inlet and outlet tends to decrease with the increase of the axial feed speed, because the cutting thickness keeps increasing with the increase of the axial feed speed, while the cutting depth remains unchanged. The axial force and radial force of ultrasonic assisted spiral grinding are increased, resulting in the difference between the actual machining aperture and the theoretical machining aperture.

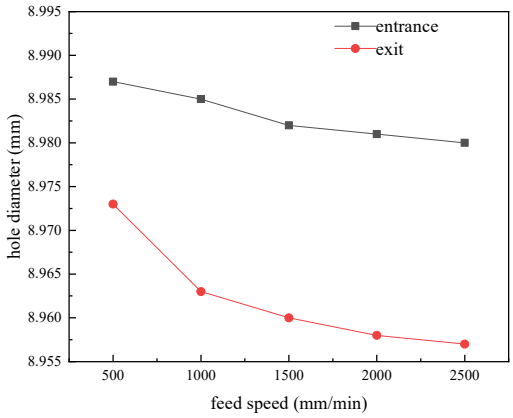

(a)e=0.5mm

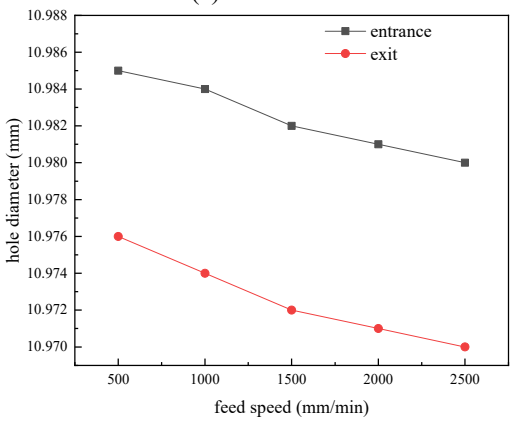

(b)e=1mm

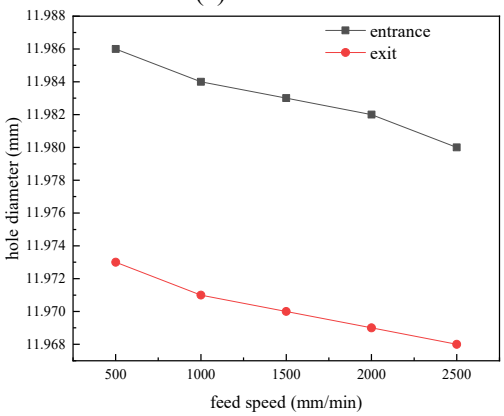

(c)e=1.5mm

Figure13 Effect of tool axial feed speed on aperture under different eccentricity

3.3.3. The influence of axial feed pitch on the dimensional accuracy of the aperture

Figure 14 shows the change curve of inlet diameter measured by axial feed pitch with different eccentricities. It can be seen from Figure15 that under the same eccentricity, due to the constant axial feed speed, the cutting thickness and cutting depth increase with the increase of the pitch, and the axial force and radial force both increase, leading to serious tool wear, resulting in the continuous reduction of inlet aperture. The aperture deviation of the inlet and outlet decreases first and then increases with the increase of eccentricity. When the eccentricity is 1mm, the aperture deviation is small.

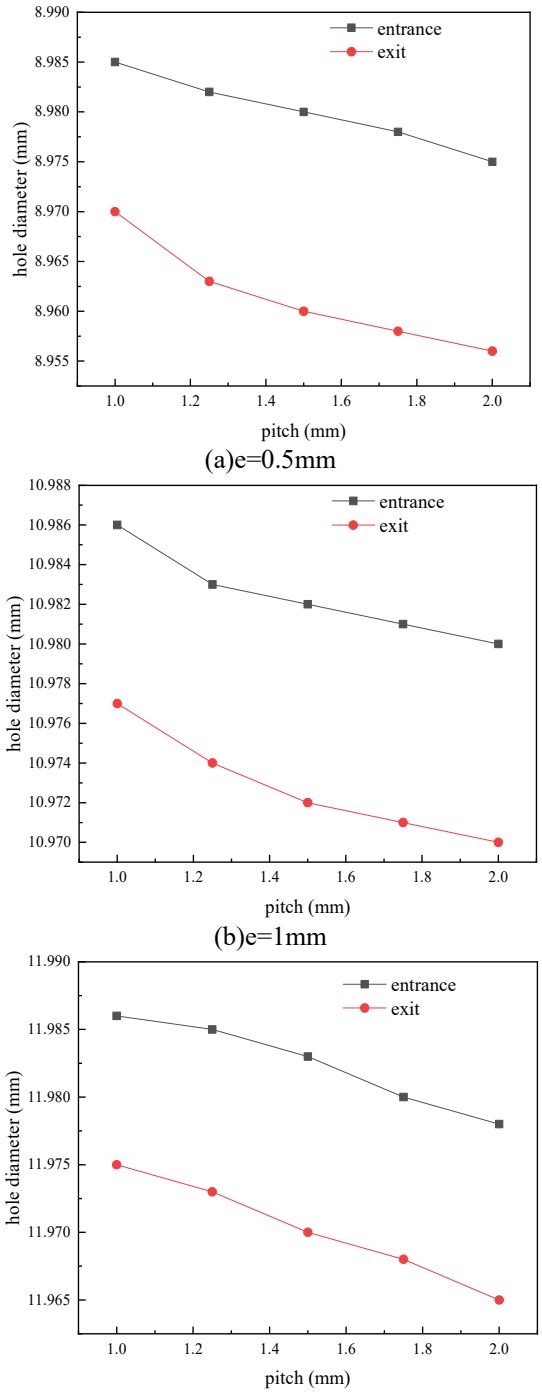

Figure 14 Influence of tool pitch on aperture under different eccentricity

In the process of spiral grinding of silicon carbide ceramics, the surface quality of the hole is mainly determined by the quality of the entrance, the quality of the exit and the surface quality of the hole wall. This experiment mainly observed the entrance of the hole, observed the appearance of the entrance of the hole after processing through a super-depth microscope, and analyzed the quality of the entrance of the machining hole. The experimental results are shown in the figure below.

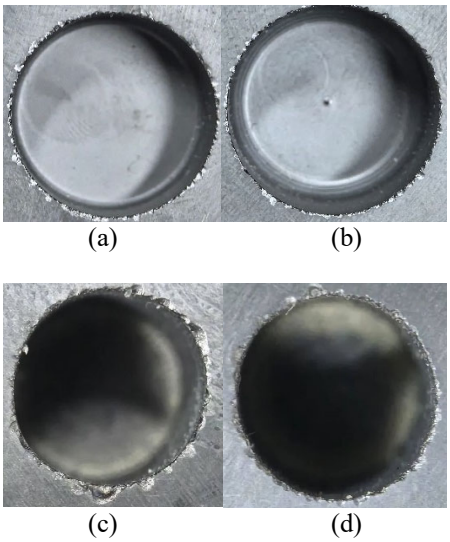

References

[1] Li Chenran, Xie Zhipeng, Kang Guoxing, et al. Research and application progress of silicon carbide ceramics at home and abroad [J]. Bulletin of Ceramics, 2020, 39(5): 1353-1370.

[2] Cao Jianguo, Zhang Qinjian. Study on Material removal characteristics of Silicon Carbide Ceramic Grinding assisted by Ultrasonic Vibration [J]. Journal of Mechanical Engineering, 2019, 55(13): 205-211.

[3] Wei J, Wang H, Lin B, et al. A force model in single grain grinding of long fiber reinforced woven composite[J]. The International Journal of Advanced Manufacturing Technology, 2019, 100: 541-552.

[4] Zhang Y, Li C, Ji H, et al. Analysis of grinding mechanics and improved predictive force model based on material-removal and plastic-stacking mechanisms[J]. International Journal of Machine Tools and Manufacture, 2017, 122: 81-97.

[5] Zhou K, Ding H H, Zhang S Y, et al. Modelling and simulation of the grinding force in rail grinding that considers the swing angle of the grinding stone[J]. Tribology International, 2019, 137: 274-288.

[6] Jiao Feng. Mechanism and experimental study of high efficiency grinding of engineering ceramics with ultrasonic assisted fixed abrasives [D]. Shanghai Jiao Tong University, 2008.

[7] Marshall D B, Lawn B R, Evans A G. Elastic/plastic indentation damage in ceramics: the lateral crack system[J]. Journal of the American Ceramic Society, 1982, 65(11): 561-566.

[8] Liu D F, Cong W L, Pei Z J, et al. A cutting force model for rotary ultrasonic machining of brittle materials[J]. International Journal of Machine Tools and Manufacture, 2012, 52(1): 77-84.